KSME

Springer

Journal of Mechanical Science and Technology 37 (7) 2023

Original Article
DOI 10.1007/s12206-023-2208-5

Keywords:
· Calibration of Raman scattering signals
· Flame structure
· Methane-air flame
· Raman spectroscopy
· Tubular flame

Correspondence to:
Dong Jin Cha
djcha@hanbat.ac.kr

Citation:
Cha, D. J. (2023). Calibration of Raman spectroscopy signals for measurements of methane-air tubular flames. Journal of Mechanical Science and Technology 37 (7) (2023) 3295~3302.
http://doi.org/10.1007/s12206-023-2208-5

Received December 31st, 2022
Revised March 4th, 2023
Accepted March 6th, 2023

† This paper was presented at International Session in KSME Annual Meeting 2022, ICC JEJU, Jeju, Korea & Online, November 9-12, 2022.
Recommended by Guest Editor Do-Nyun Kim

Calibration of Raman spectroscopy signals for measurements of methane-air tubular flames

Dong Jin Cha[1,2]

[1]Department of Building and Plant Engineering, Hanbat National University, Daejeon 34158, Korea, [2]Department of Mechanical Engineering, Vanderbilt University, Nashville, TN, 37235, USA

Abstract This paper addresses a challenging approach to calibrating visible Raman spectroscopy data when investigating laminar methane-air tubular flames, which struggles against low signal levels, signal interferences, etc. The literature study considers only the crosstalks between the CO_2 and O_2 vibrational Raman lines. This study will expand the coverage of the crosstalks from H_2 rotational Raman lines onto CO_2, O_2, N_2, and H_2O by employing four more off-diagonal elements in a calibration matrix. The matrix elements are determined using proper calibration flames and calculated compositions in their post-flame zone. The polynomials represent the calibrated temperature dependence of the non-zero matrix elements. Temperature-dependent response curves of each calibration element of this study and the literature study are then compared. It also found that most of the matrix elements in this study, when normalized by their values at room temperature, behaved very closely to those previously reported by another researcher group.

1. Introduction

Laminar tubular flames have simplified geometry suitable for studying chemical kinetics and transport processes because of their preferential diffusion effects [1]. Measuring the chemical structures of these flames, based on concentration and temperature profiles of major and minor species, enables the study of accurate, reduced chemical kinetics and molecular transport models and can be used to improve flamelet models [2] used in turbulent combustion simulations. The primary species CO_2, O_2, N_2, H_2O, and H_2 were measured by spontaneous Raman scattering in hydrogen-air premixed tubular flames, whereas the minor species OH and H were measured using laser induced fluorescence [3]. In addition, using femtosecond two-photon laser induced fluorescence (fs-TPLIF), the flame's atomic hydrogen [4] and oxygen [5] were measured. The fs-TPLIF signals were corrected for collisional quenching from major species concentrations measured by Raman scattering. Premixed tubular flames with hydrocarbon fuels such as CH_4 and C_3H_8 mixed with air were also investigated using visible laser-induced spontaneous Raman spectroscopy. The measured profiles agreed well with the investigated numerical simulations [6].

Indeed, the Raman scattering technique has wide use to measure the chemical structures of various flames, for example, planar opposed-jet flames [7, 8], premixed tubular flames [6, 9], and non-premixed opposed-flow tubular flames [10, 11]. Conventional Raman scattering still provides a wealth of information on gaseous tubular flames. There are excellent reviews of the Raman scattering technique in terms of theory and measurement in flames [12-15].

Raman scattering signals containing the signature of the molecular content of the gas mixture must be processed to determine the species concentration and temperature by accounting for the temperature dependence and crosstalk between neighboring species of Raman spectra. For example, there are crosstalks between CO_2 and O_2 vibrational Raman lines (see Fig. 6 in Ref. [6] and Fig. 8(a) in Ref. [16] for fuel-lean CH_4-air flames) and from H_2 rotational Raman

lines onto all the other species to varying degrees (see Fig. 8(b) in Ref. [16] for fuel-rich CH_4-air flames). Overlapping Raman spectra of major species also depends on the operating conditions of flames, e.g., adding diluents such as N_2 and CO_2, varying equivalence ratio, etc. It should note that the results obtained with an ultraviolet Raman source described in Ref. [16]. Raman images may contain interferences from laser induced fluorescence and broad-band flame luminescence [15].

There are two different approaches to Raman data processing: the matrix inversion method [17, 18], based on detailed calibration of the temperature-dependent system response, and the spectral fitting method [19, 20], based on libraries of theoretical spectra [15]. The former allows lower readout noises due to on-chip binning, and processing is fast, but its uncertainties in reactive species calibrations are more significant. On the other hand, the latter requires only one calibration per species and reduces uncertainty within temperature ranges that are difficult to calibrate. However, preserved spectral information comes with high readout noise, slow data acquisition rates, and significant effort to fit the Raman spectrum. A hybrid approach also combines the advantages of both methods [21].

The Raman scattering signal for i^{th} chemical species S_i can be estimated by [22],

$$S_i = E\sigma_{zz} X_i N L \Omega_\eta Q_e \Gamma(T) \lambda / (hc) \quad (1)$$

where E is the laser pulse energy, σ_{ZZ} is the vibrational Raman cross-section, X_i is the species mole fraction, N is the total number density, L is the spatial resolution along the laser beam, Ω is the quantum efficiency of the CCD camera, $\Gamma(T)$ is the temperature-dependent factor that accounts for the distribution of the molecules, λ is the wavelength, h is Planck's constant, and c is the speed of light.

In the matrix inversion method, quantitative number densities of j^{th} species N_j can be determined from a modified form of Eq. (1) as below:

$$S_i = Ef \sum_j K_{ij} N_j \quad (2)$$

where f is the experimentally-derived spatially-dependent attenuation factor, and K_{ij} is the temperature-dependent calibration matrix, representing the degree of contribution of the Raman scattering signal of j^{th} species onto that of i^{th} species. It is noted that this form is valid for a fixed detection setup; a complete formulation is discussed elsewhere [13, 17]. The gas temperature can also be given by

$$T = \frac{p_0}{k_b} \left(\sum_i N_i \right)^{-1} \quad (3)$$

where p_o is the thermodynamic pressure and k_b is Boltzmann's constant (1.38×10^{-23} J/K).

This paper reports the calibration of Raman scattering signals for measurements of methane-air tubular flames with a matrix inversion method using Raman measurements both in the near-adiabatic equilibrium region of calibration flames from a Hencken burner and in various cold gas flows. Temperature dependence of a calibration matrix element, K_{ij} in Eq. (2) represents a polynomial. While the main diagonal elements of the matrix for the flames are fixed, off-diagonal elements which relate interference from the crosstalks of the different species on the others are varied, depending on the type of the flame and the coverage degree of the crosstalk effects, as shown in Table 1. The table summarizes crosstalk elements previously employed for calibrating visible Raman scattering signals for CH_4-air flames and those used in this study. For laminar tubular flames, four more crosstalk terms, which relate interferences from H_2 rotational Raman lines onto CO_2, O_2, N_2, and H_2O species, are considered in this study in addition to those between CO_2 and O_2 vibrational Raman lines in the previous study [6, 23].

Table 1. Crosstalk elements in Raman calibration matrix for CH_4-air flames with the excitation of 532 nm Nd:YAG laser.

Researcher	Flame	Crosstalk element	Remarks
Dibble et al. (1990)	Turbulent jet flame	Ko_2ch_4, Ko_2h_2, Kh_2och_4, Kh_2ch_4	[17]
Hu and Pitz (2007, 2009)	Laminar tubular flame	Kco_2o_2, Ko_2co_2	[23, 6]
Fuest et al. (2011)	Turbulent flat flame	Kco_2o_2, Ko_2co_2, Kco_2h_2, Ko_2h_2, Kco_2h_2	[21]
This study	Laminar tubular flame	Kco_2o_2, Ko_2co_2, Kco_2h_2, Ko_2h_2, Kn_2h_2, Kh_2oh_2	-

The calibration results obtained in this study are normalized by their values at room temperature to qualitatively compare with those conducted by another research group [21]. Most of the normalized elements in the calibration matrix of the two studies agreed quite well, although the two Raman spectrometer setups are different, which would lead to different values of E, σ_{ZZ}, L, and Ω in Eq. (1). To the best of the author's knowledge, this is the comparison of calibration results of the matrix inversion method for visible Raman scattering techniques, for the first time, by two different research groups. The polynomial coefficients for the 13 non-zero elements in this study's calibration matrix are used to determine the temperature and the main species concentrations of methane-air tubular flames, which Vanderbilt University researchers will investigate; more specifically, the measured species concentrations will use to correct their collisional quenching effects against the fs-TPLIF signals collected for quantitative oxygen atom measurements in the flames.

2. Experimental setup

To better understand the calibration procedures of Raman scattering signals used in this study, the experimental apparatus consisting of a tubular burner and Raman spectroscopy

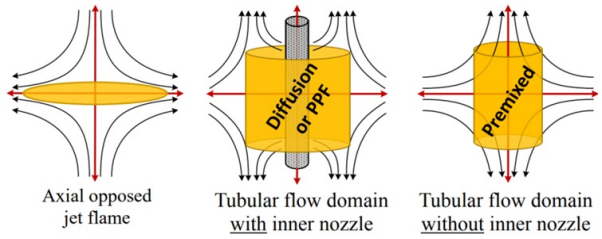

Fig. 1. Flow fields for an axial-opposed jet flame (LHS), radially-opposed jet flames with two nozzles (CTR) and a single nozzle (RHS) [25].

setup uniquely fabricated at Vanderbilt University is briefly described here. A detailed description of the setup presents in Ref. [24].

2.1 Tubular burner

The tubular burner, either premixed [6], non-premixed or diffusion [11], or partially-premixed [24], was fabricated to reduce the complexity of the combustion process from a turbulent, transient, three-dimensional problem to a laminar, steady-state, two-dimensional or one-dimensional one. As shown in Fig. 1, the tubular burner produces a radially-opposed flow field where the fluid stagnates in an axial coordinate in the form of a cylindrical face or a line. The static-in-line configuration, shown in the figure (RHS) that consists of a single inlet, the outer nozzle can be used for premixed studies while by adding an inner nozzle (CTR), a stagnant one can use on a cylindrical surface for studying pure diffusion and partially-premixed cases.

The stagnation surface radius and the stretch rate (κ) are functions of radial velocity, mixture density, and nozzle radius [26]. Tubular flames can be stabilized by a fixed stretch rate, which isolates flame stretch and curvature. The resulting laminar flames are time-independent and geometrically-simplified circumstances, leading to a two-dimensional or one-dimensional structure.

2.2 Raman spectroscopy setup

Fig. 2 shows the Raman spectroscopy setup to collect spectral data. An Nd:YAG laser was frequency-doubled (532 nm, 10 ns pulse at 10 Hz) and passed through a three-cavity pulse stretcher (cavity length ratio of 1:2:4) to reduce the peak intensity by broadening its temporal duration to 160 ns to avoid a laser-induced breakdown in the flame. Some beam reflected from a wedge window following the pulse stretcher was used to monitor the laser alignment and beam quality. The rest of the reflected beam was sent to an energy meter to measure the beam energy per pulse. The beam transmitted through the periscope was narrowed to a diameter of about 200 μm at the measuring point by a 0.3 m focal length plano-convex lens. Its energy varied from 90 to 110 mJ per pulse for the experiments.

The Raman scattering signal was collected perpendicular to the laser beam path. The signal passed through a pair of 3-inch diameter achromats (f/2 and f/7.5) and focused onto the

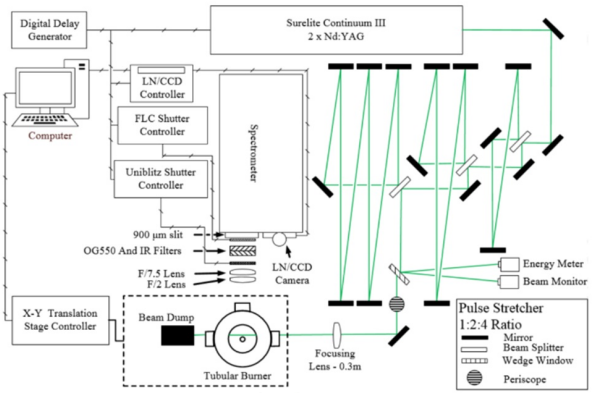

Fig. 2. Spontaneous Raman spectroscopy experimental setup [25].

slit of a modified 0.75 m Spex spectrometer (0.75 m collimating mirror and 0.65 m focusing mirror). Preceding the slit, an OG 550 filter, IR filter, optical Uniblitz shutter (6 ms opening time), and a ferroelectric liquid crystal shutter (45 μs opening time) were used to create an approximate band-pass region between 550 nm and 750 nm and reduce the exposure time to about 50 μs. Raman spectra images were captured with a liquid-nitrogen-cooled, charge-coupled camera over 600 shots, which integrates to form an image with a size of 124 pixels (spatial) by 123 pixels (spectral). Two or three Raman images were captured sequentially with different grating angles (dispersion of 0.39 mm/nm) of the spectrometer. Then it generated a full spectrum from 561.2 nm to 698.7 nm per linear scan. As a result, spatially resolved spectra were recorded along the laser line with a resolution of 86 μm, leading to an overall resolution of 200 μm for the 86 μm measurements.

3. Calibration of Raman scattering signals

For methane-air flames to be investigated, the calibration matrix K_{ij} can be constructed based on theoretical Raman spectra simulated with RAMSES [19] for seven major species CO_2, O_2, CO, N_2, CH_4, H_2O, and H_2 and for crosstalks from H_2 rotational Raman lines onto CO_2, O_2, N_2, and H_2O species and those between CO_2 and O_2 vibrational Raman lines, as shown in Eq. (4).

The main diagonal elements of the calibration matrix (calibration factors) relate the Raman scattering signals to the species number density, while its off-diagonal elements (interference factors) relate interference from the crosstalk of the different species on the others; e.g., Kco_2o_2 is the interference of the O_2 spectrum on the CO_2 Raman scattering signal. The non-zero elements in the matrix will determine in the temperature range between 300 K and 2200 K, except Kch_4. Because CH_4 readily decomposes even at moderate temperatures, the calibration factor for CH_4 is determined only in cold flows. Kch_4 is assumed to be single point calibration at room temperature and independent of temperature. This simplification justifies by the excellent agreement between experimental data and the numerical prediction [23].

Table 2. Groups of calibration flames and flow and their related elements in the calibration matrix.

Group of calibration flames and flow	Calibration matrix element
Lean H_2-air flames+cold air flow	Ko_2, Kn_2, Kh_2o, Kco_2,o_2
Rich H_2-air flames+cold H_2-air flow	Kh_2, Kco_2,h_2, Ko_2,h_2, Kn_2,h_2, Kh_2o,h_2
Lean H_2-CO_2-air flames+cold H_2-CO_2-air flow	Kco_2, Kco, Ko_2,co_2
Cold CH_4-air flow*)	Kch_4

*) A single point calibration at room temperature

Various calibration flames and flows were utilized in the calibration process. As shown in Table 2, lean H_2-air flames (ϕ_o = 0.241-0.592) and cold air flow were used to evaluate Ko_2, Kn_2, Kh_2o, and Kco_2,o_2. Rich H_2-air flames (ϕ_o = 3.583-6.355) and cold H_2-air flow were used to find Kh_2, Kco_2,h_2, Ko_2,h_2, Kn_2,h_2, Kh_2o,h_2. Lean H_2-CO_2-air flames (ϕ_o = 0.332-0.658) and cold H_2-CO_2-air flow were employed to evaluate Kco_2, Kco, and Ko_2,co_2. Cold CH_4-air flow was employed to find Kch_4.

$$K_{ij} = \begin{bmatrix} Kco_2 & Kco_2,o_2 & 0 & 0 & 0 & 0 & Kco_2,h_2 \\ Ko_2,co_2 & Ko_2 & 0 & 0 & 0 & 0 & Ko_2,h_2 \\ 0 & 0 & Kco & 0 & 0 & 0 & 0 \\ 0 & 0 & 0 & Kn_2 & 0 & 0 & Kn_2,h_2 \\ 0 & 0 & 0 & 0 & Kch_4 & 0 & 0 \\ 0 & 0 & 0 & 0 & 0 & Kh_2o & Kh_2o,h_2 \\ 0 & 0 & 0 & 0 & 0 & 0 & Kh_2 \end{bmatrix} \quad (4)$$

3.1 Calibration experiments: Raman spectra

Eq. (2) can be recast into a matrix equation *{S} = [K]{N}*, where the signal vector *{S}* is equal to $S_i/(Ef)$. The elements of the signal vector are from Raman scattering signals collected inside a 12.5 mm diameter Hencken burner flame [27]. Fig. 2 shows the calibration experiment of the Hencken burner placed the tubular burner. Hence, the optical conditions were the same between the measurement and the tubular flame experiments. Adiabatic equilibrium was assumed to be 15 mm downstream from the burner surface. Raman scattering signals were collected from the point for each flame condition, including cold conditions, as shown in Table 2. Gas flow rates to the reactants were controlled with mass flow controllers (Teledyne Hastings HFC-202/203), and co-flow rates were measured with a flow meter (Teledyne Hastings HFM-201). Flow controllers and meters are accurate to 1 % of full scale and verified by laminar flow elements.

Raman images captured for the calibration of Hencken burner flames were background-corrected, cosmic ray-cleaned, and energy-normalized before processing [28]. The Raman spectrum collected for calibration flames spans all stable major species to study methane-air flames. As shown in Table 3, the spectrum is strategically divided into spectral bins corresponding to the genuine Raman band of a particular species. The table shows the complete list of the bins used in this study,

Table 3. Spectral locations of the bins utilized on the raman camera with the excitation of 532 nm Nd:YAG laser.

Species	λ_{start} (nm)	λ_{end} (nm)
CO_2	568.3	575.8
O_2	577.6	580.9
CO	598.6	602.3
N_2	604.6	608.3
CH_4	628.5	635.0
H_2O	656.5	661.1
H_2	680.4	684.6

which is almost the same as that in Ref. [29].

Fig. 3 shows the Raman scattering signal as a function of wavelength, for the five lean H_2-CO_2-air calibration flames in Table 2, ranging from 561.2 nm to 698.7 nm. Other flames can be found in Ref. [30]. The red curves in the figure represent the vibrational Raman scattering signal intervals of the seven species for the calibration flames, as shown in Table 3. In addition, the Raman scattering signal for CH_4 was taken separately at room temperature. To calibrate the Raman scattering technique for measurements of methane-air tubular flames, the Raman scattering signals of all seven species for each calibration flame as a temperature function are now available.

3.2 Determination of calibration elements

The species number density vector *{N}* was determined by replacing the calculated species mole fractions in the post-flame zone with an adiabatic equilibrium program [31]. Fig. 4 shows the calculated temperature and mole fractions of the seven major species of the calibration flames described in Table 2. The flames were operated over various equivalence ratios to calibrate all major species. Since the mole fractions of CO and H_2 were very low, they were multiplied by 1000, as shown in Fig. 4(c). The order of magnitudes of Raman scattering signals and calculated species concentrations as a function of temperature for all the species in flames varies significantly, thus reaching threshold values for most flows (species concentration: 1×10^{16} #/cm^3). Only transgressive signals were used: the data for calibration elements ranged from 3 to 18 as a function of temperature determined for each species.

The elements in the calibration matrix, Eq. (4), both the main diagonal and off-diagonal, were obtained as polynomial functions of temperature with the {s} and {N} data specified above according to the order of the calibration flames and flow listed in Table 2. Most polynomials will determine in 1st-degree or 2nd-degree. The effect of adding four off-diagonal elements relating to H_2 rotational Raman lines on the calibration results of the other remaining elements has yet to be seen compared to those in Refs. [6, 23]. The reasons would be other experimental factors, including different ranges of equivalence ratios of calibration flames in the two calibration experiments, which may affect more significantly (not shown here).

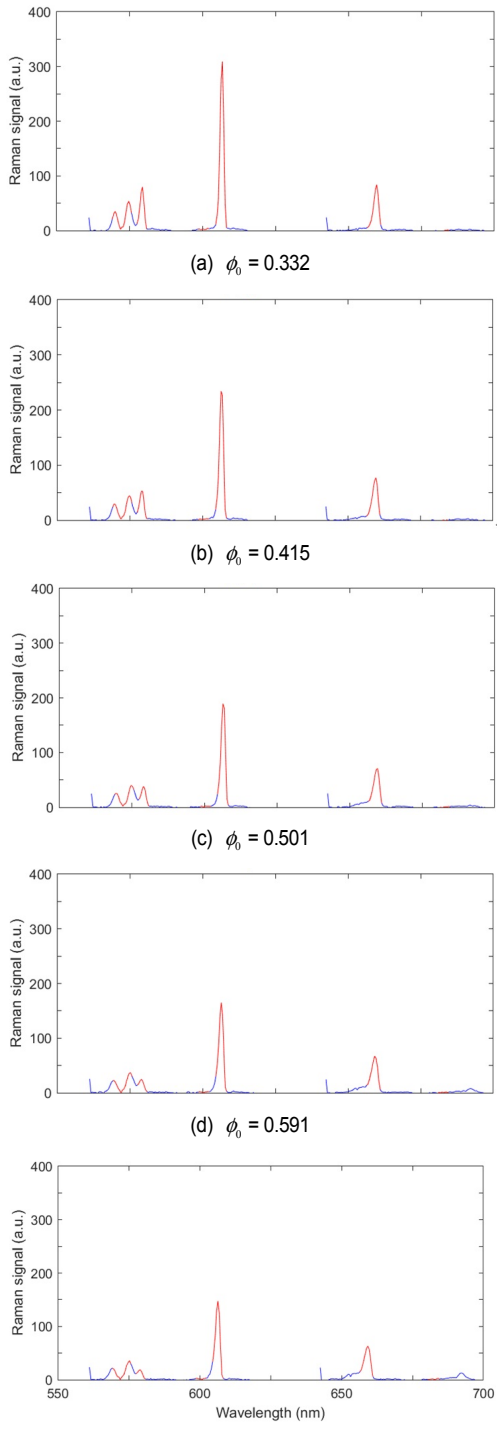

Fig. 3. Raman scattering signals of five lean H_2-CO_2-air calibration flames as a function of initial equivalence ratio.

The results of both temperature-dependent response curves, calibration and interference factors, are then normalized by their values at room temperature to qualitatively compare with similar results reported by another researcher group (see Fig. 4 in Ref. [21]).

Fig. 5(a) shows the normalized calibration factors as a function of temperature, superimposed with their curve-fittings, for the main species appearing in methane-air flames, CO_2, O_2, CO, N_2, H_2O, and H_2. Note that the magnitudes of individual response curves differ between species. The magnitude at each subplot represents relative change over the temperature range rather than absolute magnitude, as the curves normalize to unity at room temperature. For most species such as O_2, N_2, H_2O, and H_2, the overall trend of response curves investigated is quite similar to that in Ref. [21]; O_2 and N_2 show an increasing response curve, while H_2O and H_2 show decreasing response curve. For CO_2 and CO, the two results are different. The normalized Kch_4, calibrated and normalized to unity at a point at room temperature, is not included in the figure.

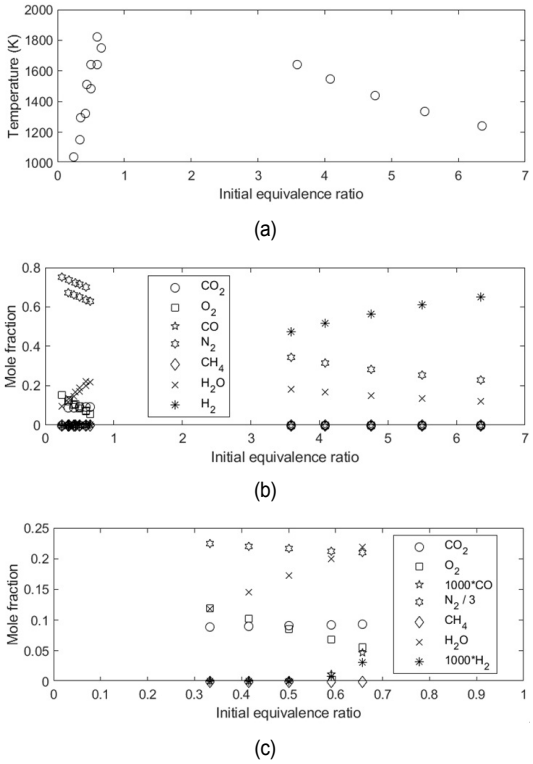

Fig. 4. Calculated (a) temperature; (b) mole fractions of seven major species of all 15 calibration flames; (c) those similar to (b) of five lean H_2-CO_2-air flames only.

Fig. 5(b) shows similar results of normalized interference factors accounting for Raman crosstalk. The sizes of most of the subplots in the figure coincide with those in Ref. [21] for better comparison. The $Kco_{2,}o_2$ curve in the figure agrees well with the reference and the $Kco_{2,}h_2$ curves in both studies show a similar increasing trend but with rather different slopes. The curves of the other off-diagonal elements are quite different from those in reference. Some factors behave differently because the calibration and interference factors affect the temperature and the Raman spectroscopy system, i.e., the optical setups in the two laboratories are different, as mentioned earlier.

The polynomial coefficients for 13 non-zero elements, including Kch_4, in the calibration matrix, were determined and will have used to measure temperature and main species concen-

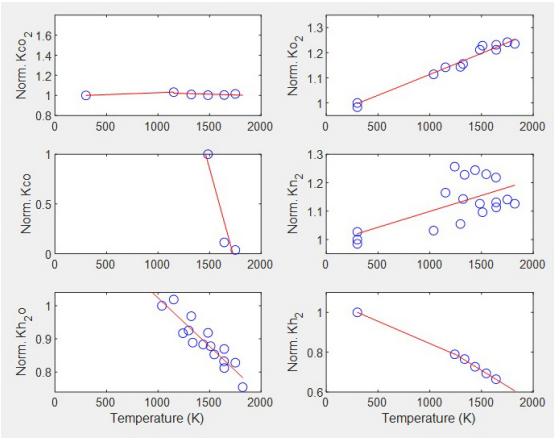

(a)

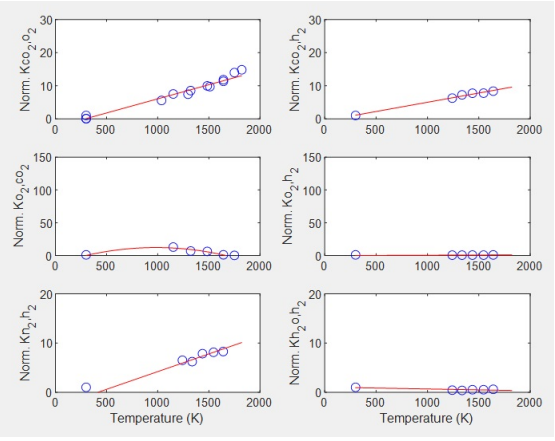

(b)

Fig. 5. (a) Normalized calibration factors of K_{ij} for CO_2, O_2, CO, N_2, H_2O, and H_2; (b) normalized interference factors of K_{ij} based on calibration polynomials (symbols show the employed fitting points).

trations in methane-air tubular flames, which Vanderbilt University researchers will soon investigate. According to a previous publication on the calibration of Raman scattering signals for hydrogen-air tubular flame measurements [30], characteristic uncertainties for chemical species are approximately ±2 % by mole fraction for hot products and ±0.5 % for room temperature reactants. However, a detailed study of the uncertainties will leave until a future publication due to the significant space required investigating the complex interplay of reduced signal levels, signal bias, etc.

4. Conclusions

An approach of calibrating visible Raman scattering data from laminar methane-air tubular flames removes the crosstalks from H_2 rotational lines onto CO_2, O_2, N_2, and H_2O by employing four more off-diagonal elements in a calibration matrix for the matrix inversion method, to the crosstalks between CO_2 and O_2 spectra considered previously. The matrix elements are determined in proper calibration experiments in cold flows and well-characterized Hencken flames, and also in the calculation of temperature and species mole fractions in the post-flame zone with an adiabatic equilibrium program. Their temperature dependence approximates as either a 1st-degree or 2nd-degree polynomial. When normalized by their values at room temperature, most of the resulting matrix elements show a reasonably close trend in temperature dependency compared to those previously reported by another research group, which validates this approach. It would be the first try to compare the calibration results of the matrix inversion method for visible Raman scattering techniques conducted by two different research groups.

The proposed approach removes undesired sources of the several crosstalks found in Raman scattering data of laminar methane-air tubular flames, which are employed to measure the chemical structure of the flames using the optical technique. Vanderbilt University researchers will measure the structure of the flames and then use the measured species concentrations to correct their collisional quenching effects against the fs-TPLIF signals collected for quantitative oxygen atom measurements in the flames. Furthermore, the measured temperature and species concentrations will compare to numerical predictions using different, detailed chemical kinetic mechanisms. This will further attempt to correlate the chemical kinetics of methane-air tubular flames as functions of combustion-based non-dimensional numbers. However, it may be desirable to perform both a systematic uncertainty analysis and a sensitivity analysis of calibration elements to confirm the validity and effects of the calibration element on the accuracy of the method used in this study.

Acknowledgments

This work was supported by the International Collaborative Research Program of Hanbat National University, which granted financial resources from the Ministry of Education, the Republic of Korea in 2022. The author is grateful to Prof. Robert W. Pitz at Vanderbilt University for providing his invaluable experimental data and fruitful discussions.

Nomenclature

c	: Speed of light
E	: Laser pulse energy
f	: Attenuation factor
h	: Plank's constant
i,j	: Indices
k	: Boltzmann's constant
K	: Calibration coefficient matrix
L	: Spatial resolution along laser beam
N	: Total number density
Q	: Quantum efficiency of a CCD camera
S	: Raman scattering signal
T	: Temperature
X	: Species mole fraction
η	: Efficiency of a detection system
κ	: Stretch rate
λ	: Wavelength

σ : Vibrational Raman cross section
Γ : Factor that accounts for distribution of the molecules
Ω : Collection solid angle

References

[1] R. W. Pitz, S. Hu and P. Y. Wang, Tubular premixed and diffusion flames: effects of stretch and curvature, *Progress in Energy and Combustion Science*, 42 (1) (2014) 1-34.

[2] M. S. Sweeney, S. Hochgreb, M. J. Dunn and R. S. Barlow, Multiply conditioned analyses of stratification in highly swirling methane/air flames, *Combustion and Flame*, 160 (2013) 322-334.

[3] C. A. Hall and R. W. Pitz, Modeling of cellular tubular flames, *Combustion Theory and Modelling*, 20 (2) (2016) 328-348.

[4] C. A. Hall, W. D. Kulatilaka, N. Jiang, J. R. Gord and R. W. Pitz, Minor species structure of premixed cellular tubular flames, *Proceedings of the Combustion Institute*, 35 (2015) 1107-1114.

[5] G. M. Marshall, P. S. Walsh and R. W. Pitz, Quantitative oxygen atom measurements in lean, premixed, H_2 tubular flames, *Proceedings of the Combustion Institute*, 38 (2021) 1833-1841.

[6] S. T. Hu, P. Y. Wang and R. W. Pitz, A structure study of premixed tubular flames, *Proceedings of the Combustion Institute*, 35 (2009) 1133-1140.

[7] D. Tree, T. M. Brown, K. Seshadri, M. D. Smooke, G. Balakrishnan, R. W. Pitz, V. Giovangigli and S. P. Nandula, The structure of nonpremixed hydrogen-air flames, *Combustion Science and Technology*, 104 (1995) 427-439.

[8] J. A. Wehrmeyer, Z. X. Cheng, D. M. Mosbacher, R. W. Pitz and R. J. Osborne, Opposed jet flames of lean or rich premixed propane-air reactants versus hot products, *Combustion and Flame*, 128 (3) (2002) 232-241.

[9] D. M. Mosbacher, J. A. Wehrmeyer, R. W. Pitz, C. J. Sung and J. L. Byrd, Experimental and numerical investigation of premixed tubular flames, *Proceedings of the Combustion Institute*, 29 (2002) 1479-1486.

[10] S. T. Hu, P. Y. Wang, R. W. Pitz and M. D. Smooke, Experimental and numerical investigation of non-premixed tubular flames, *Proceedings of the Combustion Institute*, 31 (2007) 1093-1099.

[11] S. T. Hu and R. W. Pitz, Structure study of non-premixed tubular hydrocarbon flames, *Combustion and Flame*, 156 (1) (2009) 51-61.

[12] D. A. Long, *Raman Spectroscopy*, McGraw-Hill, New York, USA (1977).

[13] A. C. Eckbreth, *Laser Diagnostics for Combustion Temperature and Species*, 2nd Ed., Gordon and Breach Publishers, United Kingdom (1996).

[14] K. Kohse-Hoinghaus and J. Jeffries, *Applied Combustion Diagnostics*, Taylor and Francis, New York, USA (2002).

[15] W. Meier and T. Seeger, Laser Raman scattering, A. Steinburg and S. Roy (Eds.), *Optical Diagnostics for Reacting and Non-Reacting Flows: Theory and Practice*, American Institute of Aeronautics and Astronautics, Inc. (2023) 137-179.

[16] J. A. Wehrmeyer, T.-S. Cheng and R. W. Pitz, Raman scattering measurements in flames using a tunable KrF excimer laser, *Applied Optics*, 31 (10) (1992) 1495-1504.

[17] R. W. Dibble, S. H. Starner, A. R. Masri and R. S. Barlow, An improved method of data acquisition and reduction for laser Raman-Rayleigh and fluorescence scattering from multispecies, *Applied Physics B*, 51 (1990) 39-43.

[18] R. S. Barlow, C. D. Carter and R. W. Pitz, Multiscalar diagnostics in turbulent flames, K. Kohse-Hoinghaus and J. Jeffries (Eds.), *Applied Combustion Diagnostics*, Taylor and Francis, New York, USA (2002).

[19] D. Geyer, 1D Raman/Rayleigh experiments in a turbulent opposed jet, *Ph.D. Thesis*, TU Darmstadt, Dusseldorf, Germany (2005).

[20] J. Kosima and Q.-V. Nguyen, Quantitative analysis of spectral interference of spontaneous Raman scattering in high-pressure fuel-rich H_2-air combustion, *Journal of Quantitative Spectroscopy and Radiative Transfer*, 94 (2005) 439-466.

[21] F. Fuest, R. S. Barlow, D. Geyer, F. Seffrin and A. Dreizler, A hybrid method for data evaluation in 1-D Raman spectroscopy, *Proceedings of the Combustion Institute*, 33 (2011) 815-822.

[22] R. W. Pitz, Raman spectroscopic measurements of tubular flames, S. Ishizuka et al. (Eds.), *Tubular Combustion*, Momentum Press, LCC, New York, USA (2013).

[23] S. Hu, Measurements and modeling of non-premixed tubular flames: structure, extinction and instability*, Ph.D. Thesis*, Vanderbilt University, Nashville, TN (2007).

[24] D. C. Tinker, C. A. Hall and R. W. Pitz, Measurement and simulation of partially-premixed cellular tubular flames, *Proceedings of the Combustion Institute*, 37 (2019) 2021-2028.

[25] D. C. Tinker, C. A. Hall and R. W. Pitz, Major species measurement and simulation of partially-premixed, cellular, tubular H_2-air flames, *55th AIAA Aerospace Sciences Meeting,* Grapevine, Texas, USA (2017).

[26] P. Wang, J. A. Wehrmeyer and R. W. Pitz, Stretch rate of tubular premixed flames, *Combustion and Flame*, 145 (1-2) (2006) 401-414.

[27] P. Wang, X. Luo and Q. Li, Heat transfer study of the Hencken burner flame, *Flow Turbulence Combustion*, 101 (2018) 795-819.

[28] R. J. Osborne, P. A. Skaggs and R. W. Pitz, Multi-camera /spectrometer design for instantaneous line Rayleigh/Raman /LIPF measurements in methane/air flames, *34th AIAA Aerospace Sciences Meeting*, Reno, Nevada, USA (1996).

[29] M. J. Dunn, A. R. W. Macfarlane, R. S. Barlow, D. Geyer, K. Dieter and A. R. Masri, Spontaneous Raman-LIF-CO-OH measurements of species concentration in turbulent spray flames, *Proceedings of the Combustion Institute*, 38 (2021) 1779-1786.

[30] D. J. Cha, D. C. Tinker, C. A. Hall and R. W. Pitz, Reduction of Raman spectroscopy data for H_2-CO_2-air tubular flame measurements, *Journal of Korean Society of Combustion*, 27 (2) (2022) 1-13.

[31] D. Goodwin, H. K. Moffat and R. L. Speth, *Cantera: An Object-Oriented Software Toolkit for Chemical Kinetics, Thermodynamics, and Transport Processes*, Version 2.2.0 (2015) doi: 10.5281/zenodo.48735.

Dong Jin Cha is a Building and Plant Engineering Professor at Hanbat National University in Daejeon, Korea and an Adjoint Professor of Mechanical Engineering at Vanderbilt University in Nashville, TN, USA. He received his Ph.D. in Mechanical Engineering from the University of Illinois at Chicago, IL, USA. His research interests include combustion instability in gas turbines for power generation and fluid flows in building and plant engineering.